Vibrational spectroscopy of hydrogens in diamond: A quantum mechanical treatment

(Article begins on next page)

28 July 2024

Can hydrogen atoms saturate the four dangling bonds of the carbon atoms around the vacancy in diamond? A Quantum Mechanical investigation.

Francesco Silvio Gentile,[1] Simone Salustro,[1] Jacques Kontak
Desmarais,[1] Anna Maria Ferrari,[1] Silvia Casassa,[1] and Roberto Dovesi[1]

[1]*Dipartimento di Chimica, Università di Torino and*
NIS (Nanostructured Interfaces and Surfaces) Centre,
Via P. Giuria 5, 10125 Torino, Italy

1

Abstract

aggiungere il bending e altre 2 limitations

VH_n ($n=1$ to 4) defects in diamond (hydrogen atoms saturating the dangling bonds of the carbon atoms surrounding a vacancy) are investigated at the quantum mechanical level by using the periodic supercell approach, an *all electron* gaussian type basis set, "hybrid" functionals, and the CRYSTAL code. Most of the results have been collected for S_{64} (a supercell containing 64 atoms). However, for the cases with the highest H concentration, VH_4, also the S_{216}, S_{512} and S_{1000} supercells have been considered, to explore the effect of the defect concentration on the IR and Raman spectra. Various spin states are considered ($S_z = 1/2$ for VH_1; $S_z = 1$ and 0 for VH_2 and V, the pure vacancy, here included for comparison; $S_z = 1/2$ and $3/2$ for VH_3 and $S_z = 0$ for VH_4): their relative stability, band structure, charge and spin density distributions are analyzed. All the investigated systems present specific IR and Raman spectra, with peaks that can be used for the characterization of the defects. In particular the CH stretching peaks can be considered fingerprints of the system: they range (when anharmonicity is taken into account) from 2500 to 4400 cm^{-1} as a function of the number of H atoms in the vacancy. Also the dependence on the spin state is remarkable: for VH_1, its harmonic frequency increases from about 2800 cm^{-1} for the quadruplet state to about 3200 cm^{-1} for the doublet. The accurate determination of these vibrational frequencies requires two main ingredients, that have been used in the present study: i) "hybrid" functionals, that are known to produce accurate vibrational frequencies; ii) a specific treatment for the determination of the stretching CH anharmonicity. The latter too is extremely sensitive to the H load and spin state of the system, ranging from -340 cm^{-1} (the lowering of the wavenumber with respect to the harmonic value in VH_1) to +84 cm^{-1} for VH_4, where the anharmonic wavenumber increases with respect to the harmonic value due to the strong repulsion with the other H atoms. The graphical animation of the modes (see `http://www.pmmp.jussieu.fr/yves/defectsindiamond/`) permits to investigate the nature of the full set of modes.

Keywords: Diamond, 1 to 4 H in the vacancy, electronic structure, formation energy, IR spectrum, anharmonicity, animation of the vibrational modes, isotopic substitution

I. INTRODUCTION

aggiungere il bending

Hydrogen is one of the most important impurities in diamond. It is included during the growth of natural diamond as well as in chemical vapour deposition (CVD) processes. It is certainly present at the surfaces; a non minor fraction, however, is also thought to be incorporated in the bulk. H atoms are supposed to be present in several defects[1,2], involving vacancies and/or nitrogen atoms isolated or aggregated. It is mostly identified through its infrared (IR) active modes (stretching and bending), although probably not all hydrogen atoms present in diamond are IR active. A general review concerning hydrogen in diamond has been published in 2002 by Briddon and coworkers[3], that explores a set of hydrogen containing defects from the simulation point of view. Five years later a second review paper appeared[4], that gives an overview, from the experimental side, of the peaks that "*have been at least tentatively attributed to H-related defects*".[4] As a matter of fact, the one to one correspondence between the many peaks that can reasonably be attributed to H (some of the wavenumbers larger than say 1400 cm^{-1}) and a specific local defect is still lacking. For example, only very recently (in 2014) Briddon and coworkers have been able to attribute to the VN$_3$H defect[5] (a vacancy surrounded by three N and a C atoms saturated by H) the peaks at 1405 and 3107 cm^{-1}, that are observed in almost all types of Ia natural diamonds[1,4,6–8]. In particular, and with reference to the present investigation, we have been unable to find indications concerning the number of H atoms that can *enter* in the vacancy: is there enough *space* for two, or three, or four H atoms saturating the C dangling bonds? Do the progressive saturation remain exothermic up to 3 or 4 H atoms, or is the steric hindrance preventing the high loading? How different is the IR spectrum of the various VH$_n$ compounds and spin states? Is the Raman spectrum adding complementary information?
From the experimental side, it is obviously very difficult to know how many different defects containing H are present, and at which concentration, and how combined with other defects. From the simulation point of view, where it is possible to define *a priori* the kind of defects present in the bulk, other limitations prevent however from a simple identification of the experimental peaks. The four most important limitations are related to a) the use of functionals (LDA, GGA) that are known to perform poorly with open shell systems, and in

describing H atoms for which the self interaction error is particularly severe[9]; b) inaccuracies in the models for treating the vibrational modes, that in the particular case of the C-H stretching is very anharmonic; c) the non availability of the IR intensities, that permit to complement the wavenumber calculation for producing the full spectrum and d) difficulties in modeling large unit cells or clusters, under the hypothesis that the experimental data refer to "isolated" defects, where the mutual interaction is supposed to be negligible. Some of these limitations deeply affect the previous quantum mechanical simulations of H containing defects.

Here we extend our preliminary investigation devoted to VH_1[10], by considering the full set of VH_n (n= 1 to 4) defects, with significant improvements with respect to previous treatments (the four limitations mentioned above are totally or in part eliminated). One, two, three and four dangling bonds of V (the diamond vacancy) are saturated, by using a supercell approach, hybrid functionals (most of the calculations will be performed with B3LYP), a Gaussian type basis set and the supercell scheme. Cells containing 64 atoms, S_{64}, have been considered. However, for the cases with highest H concentrations (VH_4), for which the defect-defect interaction might be important, also the S_{216}, S_{512} and S_{1000} supercells have been investigated. It is worth noting that S_{1000} is by far the largest supercell for which the vibrational spectrum and the IR intensities have been computed.

Various spin states are considered ($S_z = \frac{1}{2}$ and $\frac{3}{2}$ for VH_1; $S_z = 1$ and 0 for VH_2 and V, the pure vacancy, here included for comparison; $S_z = 1/2$ for VH_3 and $S_z = 0$ for VH_4): their relative stability, band structure, charge and spin density distributions are analyzed. All the investigated systems present specific IR spectra, with peaks that can be used for the characterization of the defects. In particular the C-H stretching peaks can be considered fingerprints of the system: they range (when anharmonicity is taken into account) from 2500 to 4400 cm^{-1} as a function of the number of H atoms in the vacancy. Anaharmonicity is extremely sensitive as well to the H load and spin state of the system, ranging from 340 cm^{-1} (the lowering of the wavenumber with respect to the harmonic value in VH_1) to -84 cm^{-1} for VH_4, where the anharmonic wavenumber increases with respect to the harmonic value due to the strong repulsion with the other H atoms. The graphical animation (see `http://www.pmmp.jussieu.fr/yves/defectsindiamond/`) permits to investigate the nature of the full set of modes.

The paper is structured as follows. In Section II information on the adopted method is pro-

vided. Subsection II A is devoted to the vibrational frequencies computed in the harmonic approximation, and to the analytical estimation of the IR and Raman intensities. Subsection II B illustrates how the anharmonic contribution to the stretching is computed by solving numerically the corresponding one dimensional Schroedinger equation. Section III is organized in two parts. Subsection III A is devoted to the equilibrium geometry of the defect, to its charge distribution and to the band structure. In Subsection III B, the vibrational features of the defect are reported and analyzed, both at the harmonic and anharmonic level; comparison with experimental findings and previous simulations is performed. Finally, in Section IV some conclusions are drawn.

II. COMPUTATIONAL MODELS AND DETAILS

Calculations have been performed by use of the B3LYP global hybrid functional,[11,12] as implemented in the CRYSTAL program.[13] An all-electron basis set of Gaussian-type functions has been adopted (Pople's 6-21G) for carbon, whose exponent of the most diffuse sp shell is 0.23 Bohr^{-2}. For hydrogen, the basis set of the 6-31G set has been used.[14] The defect formation energy and the C-H anharmonic vibrational frequency have also been calculated with larger basis sets (6-21G*, 6-31G and 6-31G*[15]) and other functionals, ranging from pure (LDA[16] and PBE[17]), to global (PBE0[18]), and range-separated (HSE06[19]) hybrids. The truncation of the Coulomb and exchange infinite lattice series is controlled by five thresholds T_i (see CRYSTAL manual, Ref. 20, for more details), which have been set to 8 (T_1-T_4) and 16 (T_5). The convergence threshold on energy for the self-consistent-field (SCF) procedure has been set to 10^{-8} Hartree for structural optimizations and to 10^{-10} Hartree for vibration frequency calculations.

The DFT exchange-correlation contribution to the Fock matrix has been evaluated by numerical integration over the unit cell volume. Radial and angular points for the integration grid are generated through Gauss-Legendre radial quadrature and Lebedev two-dimensional angular point distributions. The default pruned grid with 75 radial and 974 angular points has been used, whose accuracy can be measured by comparing the integrated charge density in the largest supercell here considered (128 atoms), $N_i = 770.011$, with the total number of 770 electrons in the unit cell.

A periodic supercell approach is used to simulate different defect concentrations. Supercells

containing 64 and 128 atoms have been considered (to be referred to in the following as S_n, with $n=$ 64 or 128). In the V_4 case, for exploring the effect of larger dilutions of the defect on the IR spectrum, also the S_{256}, S_{512} and S_{1000} supercells have been considered. Reciprocal space has been sampled using a regular sub-lattice, centered at the origin ($\Gamma point$), with a shrinking factor of 8 for S_{64}, 4 for S_{128}, and 2 for the larger supercells, which corresponds to a sampling over xx (S_{64}) and 13 (S_{128}) and zz (S_{216}, S_{512} and S_{1000}) **k**-points in the irreducible part of the Brillouin zone for the case with highest symmetry (VH_4).

A. Harmonic frequencies and the IR and Raman spectra

Frequencies at the Γ point are obtained within the harmonic approximation by diagonalising the mass-weighted Hessian matrix, W, whose elements are defined as[21–25]

$$W^{\Gamma}_{\alpha i,\beta j} = \frac{H^{\mathbf{0}}_{\alpha i,\beta j}}{\sqrt{M_\alpha M_\beta}} \quad \text{with} \quad H^{\mathbf{0}}_{\alpha i,\beta j} = \left(\frac{\partial^2 E}{\partial u^{\mathbf{0}}_{\alpha i} \partial u^{\mathbf{0}}_{\beta j}} \right) , \tag{1}$$

where M_α and M_β are the masses of atoms associated with the i and j atomic coordinates. Once the Hessian matrix, $\mathcal{H}_{\alpha i,\beta j}$, has been calculated, frequency shifts due to isotopic substitutions can be calculated readily, at no computational cost, by changing masses in Eq. 1. Energy first derivatives with respect to the atomic positions, $v_{\alpha,j} = \partial E / \partial u_{\alpha,j}$, are calculated analitically for all the $u_{\alpha,j}$ coordinates (E is the total energy, $u_{\alpha,j}$ is the displacement coordinate with respect to the equilibrium, α labels each atom), whereas second derivatives at $\vec{u} = 0$ are calculated numerically using a single displacement along each coordinate ($N=2$, the central point and a point on the positive side):

$$\left[\frac{\partial v_{\alpha j}}{\partial u_{\beta i}} \right] \approx \frac{v_{\alpha j}(0, \ldots, u_{\beta i}, \ldots)}{u_{\beta i}} \tag{2}$$

or averaging two displacements ($N=3$):

$$\left[\frac{\partial v_{\alpha j}}{\partial u_{\beta i}} \right] \approx \frac{v_{\alpha j}(0, \ldots, u_{\beta i}, \ldots) - v_{\alpha j}(0, \ldots, -u_{\beta i}, \ldots)}{2u_{\beta i}} \tag{3}$$

Previous calculations[21,26,27] have shown that in bulk systems the influence of both u and N is very small (less than 1 cm^{-1}) when H atoms are not present; much larger effects have been found for katoite[28], brucite[29,30] and diaspore[31], related to the anharmonicity of the O-H stretching. More generally, anharmonicity is large in all cases in which H atoms are

involved (*vide infra*)[32,33]. Integrated intensities for IR absorption $\mathcal{I}_p$ are computed for each mode p by means of the mass-weighted effective-mode Born-charge vector $\vec{Z}_p$[34,35] evaluated through a CPHF/KS approach:[36,37]

$$\mathcal{I}_p \propto \left| \vec{Z}_p \right|^2 . \tag{4}$$

The relative Raman intensities of the peaks are computed analytically by exploiting a scheme illustrated in Refs. 38,39. Both schemes are based on the solutions of first- and second-order Coupled-Perturbed-Hartree-Fock/Kohn-Sham (CPHF/KS) equations.[40,41]

B. The anharmonicity of the C-H stretching mode

When both the fundamental frequency ω_{01} and the first overtone ω_{02} of a mode are available, the anharmonicity constant $\omega_e \chi_e$ can be obtained through the formula (see Ref. 30 for more details):

$$\omega_e \chi_e = \frac{(2\omega_{01} - \omega_{02})}{2} \tag{5}$$

that permits also the definition of the harmonic frequency ω_e as:

$$\omega_e = \omega_{01} + 2\omega_e \chi_e \tag{6}$$

The importance of anharmonicity in H containing systems is clear by looking at the anharmonicity constant $\omega_e \chi_e$ of some simple diatomic molecules such as H_2, HF, HCl and HBr where $\omega_e \chi_e$ is 121, 90, 53 and 45 cm^{-1}, respectively[42]. For the O-H stretching, the anharmonicity can reach 200 cm^{-1}, or even more when O-H is involved in strong hydrogen bonds[29,32]. As regards the C-H stretching, anharmonicity is estimated to be around 120-140 cm^{-1} for many organic molecules[43,44].

The very large anharmonicity of the C-H, N-H and O-H stretching modes can be estimated taking advantage of their independence from the other normal modes.[27–29,33]

A scheme has been implemented in the CRYSTAL code that solves numerically the one-dimensional Schrödinger equation when the potential energy, evaluated at 7 points along the C-H coordinate, is fitted with a sixth order polynomial.[45] The explored interval for the present case goes from -0.8 to +1.0 Å from the equilibrium position. The explored energy range is about 1.1 eV. The results vary by less than 1 cm^{-1} when a much richer set of points (26) is used in the same interval.

Unfortunately this simple and effective scheme cannot be extended to the other vibrational modes involving hydrogen, such as bending, because in this case the separability with respect to the other modes is lost. In this case a full anharmonic treatment is required, that is not yet available in the CRYSTAL code.

III. RESULTS

Let us summarize the electronic situation of the systems we are considering in the present study. In the vacancy V there are 4 uncoupled electrons, that can generate three different states characterized by $S_z=0$, 1 and 2 (four spin up, three up and one down, two up and two down); we can call these states quintuplet, triplet and singlet, although only the first one is a pure spin state of the S^2 operator. It should be underlined that the unpaired electrons remain localized to a large amount on the carbon atoms, as it should be, if and only if a large enough amount of "exact" Hartree-Fock (HF) exchange is included in the functional. With the HF method the localization is complete (one electron on each carbon atom); in "hybrid" functionals, such as B3LYP or PBE0 (very rarely adopted in previous studies for these systems), the localization remains large (about 0.8 $|e|$ on each dangling carbon bond, according to a Mulliken partition of the charge density). LDA and various versions of GGA, like PBE, are unable to localize these electrons, and the solution turns out, for many of the defects in diamond, to be metallic, in contrast with experimental evidence. The energy difference between the singlet and triplet states of the vacancy, evaluated at the B3LYP/6-21G level, is quite small (0.13 eV), whereas the quintuplet is less stable by about 1.4 eV.[46,47]

The dangling bonds are progressively saturated by hydrogen atoms, so that in VH$_1$ the three uncoupled electrons can generate a quadruplet (q, $S_z=3/2$) or a doublet (d, $S_z=1/2$); in VH$_2$ the two unpaired electrons can generate a triplet (t, $S_z=1$) or a singlet (s, $S_z=0$). In VH$_3$ the only unpaired electron is in a doublet state ($S_z=1/2$). Finally, in VH$_4$ there are no uncoupled electrons and the ground state is a closed shell. The relative stability of the different spin states, and the stability of the various defects when the number of hydrogen atoms in the vacancy is increasing, are among the issues that will be discussed in this Section.

A. Geometry, charge and spin densities, band structure and the C-H homolytic dissociation

The geometry is relatively similar for the various cases here considered. As we are mainly interested in the behavior of the C-H groups, we reported in Table I only two geometrical data, namely the C-H and the H-H distances (when applies). The former is equal to 1.07 Å when a single H atom is present (in the low spin VH_1^d state) , to 1.05 Å when there are two H atoms in the cavity, to 1.03 Å in the case with three H atoms, and to 1.01 Å in VH_4, as a consequence of the respulsion between hydrogen atoms. In the high spin VH_1^q state, with 3 spin up electrons, the C-H distance is longer (1.10 Å),than in VH_1^d as a consequence of the strong Pauli repulsion due to the uncoupled electrons on the three carbon atoms.

The H-H distance is 1.27 Å in the cases with 2 and 3 H atoms, and reduces to 1.25 Å in VH_4, due to the HH repulsion. The polarity of the C-H bond is large when a single or two H atoms are present (+0.17 $|e|$ on H and -0.15 to -0.13 $|e|$ on C_1); it reduces progressively when the number of H atoms increases (+0.12 and -0.10 $|e|$ in VH_3, +0.07 and -0.04 $|e|$ in VH_4) so as to reduce the reciprocal repulsion among them. When the system is spin polarized, the spin density is essentially localized on the unsaturated C atoms (the magnetic moment of these C atoms is about 0.8 $|e|$): Table I shows that the amount of spin density on H and C_1 is very small, the maximum being +0.17 $|e|$ on C_1 (a C atom linked to H) for a system with three uncoupled electrons (the VH_1^d case); the magnetic moment of H is in all cases close to zero. The C-H bond population increases from 0.27 to 0.31 $|e|$ from VH_1 to VH_3, in parallel to the shortening of the C-H distance. In VH_4, however, it slightly decreases. The H-H bond population is negative (repulsive) and increases progressively up to -0.10 $|e|$, a quite non negligible value, in VH_4.

Bi-dimentional density maps, representing the Mulliken α-β spin population, have been plotted for all open shell S_{64} supercell systems in order to highlight the spin momentum density localized over the carbon atoms with the unpaired electrons. For all VH_x systems in d, q, s and t states the planes have been selected using symmetry criterion, involving the unsaturated carbon atoms. In quadruplet configuration of the VH_1 system the three carbon atoms (C_B,C_C,C_D in Figure 1) with their unpaired electron are symmmetry equivalent (C_{3v} point group) and the selected plane includes two of these unsaturated carbon and the H_1 hydrogen atoms. For the doublet configuration (σ_v P.G.) we have two carbon atoms (C_B

and C_C in Figure 1), symmetry equivalent, with same spin orientations and an other carbon (C_D in Figure 1) with opposite spin momentum. In order to underline the spin pecularity of this system two different planes have been selected; one plane contains the C_B, C_D (with opposite spin) and the H_1 atoms, while the other plane includes the C_B, C_C (with same spin) and the hydrogen H_1. In the VH_2 system in the triplet state (C_s point group) there are two unsaturated carbon atoms (C_C and C_D in Figure 1) with same spin configuarations, while in singlet state (C_1 point group) that carbon atoms have an opposite spin. In both systems an identical plane has been choosen and it includes the C_A, H_1 and H_2 atoms and it corresponds to the σ_v mirror plane defined in triplet configuration. In the last VH_3^d system (C_{3v}) the plane selected contains C_A, C_B and H_1 atoms and it includes the unpaired electron localized on the C_D carbon atom. The maps are shown in Figure 2 and in all cases the common aspect consists in the large localization of the spin density over the unsaturated carbon and an extented effect to the second atomic neighbours. The density polarization is more evident, in particular, for the quadruplet and triplet configurations: indeed this effect is due to the Pauli repulsion of the electrons involved in the adiacent unsaturated carbon atoms with same spin. In fact in the doublet and singlet states, for the alternation of α and β electrons, the short range repulsions are rather reduced with a consequent energy lowering. The polarizition of spin density localized over the Hydrogen atoms is gradually decreased in the high spin configurations when the H-saturation increasing, while in low spin states is almost null (including the VH_3^d case).

The band structure of the systems and states here investigated are shown in Figure 3, where the energy levels associated to α and β electrons are represented by continuous black and dotted red lines, respectively. All the investigated systems but VH_4 have an open-shell ground state. The gap range of the explored configurations grows when the number of hydrogen increases, and it has an upper limit in the pristine diamond gap value (5.76 eV). For VH_4 it is 5.67 eV. In all other cases, defect bands related to the uncoupled electrons are present in the gap. In these cases the reference lowest difference between HOCO and LUCO are the singlet (1.64 eV) and triplet states (1.37 eV) of the pure vacancy. The number of the states situated in the diamond gap reduces as a consequence of hydrogen saturation, as the energy levels of the electrons in the band referred to a C-H bond fall down in the occupied manifold.

In the VH_1 case (three uncoupled electrons), the three energy levels appearing in the gap

just below the Fermi energy (marked by the horizontal blue line) are two α and one β for the doublet, and three α for the quadruplet. In VH_2 (two uncoupled electrons), there are one α and one β band under the Fermi levels for the singlet, and two α bands for the triplet. In VH_3, there is a single uncoupled electron, with one α electron below the Fermi level. The energy dispersion of the levels occupied by the unpaired electrons is slightly smaller than 1.0 eV for all spin states with the 64 atoms supercell, and is a measure of the interaction between defects belonging to different cells. When the supercells sizes increase, and then the defect concentrations reduces, the energy dispersion reduces too.[10] In Figure 3 two different energy transitions are reported, both starting from the Γ-point. The first transition, which is a vertical one (turquoise arrow), involves the highest occupied level of the defect and the first unoccupied level of the diamond host. The second transition involves the last occupied and the first unoccupied energy levels of the defective states. These last transitions are reported with black and red arrows for α or β transitions.

In Table II the energy required for the homolytic dissociation (E_H) of the VH_x is reported, in agreement with the following reaction:

$$VH_x \rightleftharpoons V^s + \frac{x}{2}H_2 \tag{7}$$

The s (singlet) superscript refers to the most stable state of the vacancy. These reactions, corresponding to the progressive saturation of the four dangling bonds in the vacancy, are always exothermic also when reference is done to half the energy of the H_2 molecule (-0.5844 hartree). The energy would be higher by 2.31 eV per H atom if reference would be done to atomic H (-0.4969 hartree, when the same basis set and functionals are used). Table II shows that, when the progressive insertion of hydrogen is considered, the energy gain is rapidly reducing, from 1.06 eV, then to 0.72 eV (1.78-1.06) and to 0.33 eV (2.11 eV for VH_3 minus 1.78 eV for VH_2^s; the insertion of the last H atom is unfavorable by 0.02 eV when reference is done to the H_2 molecule (it remains however favorable by 2.29 eV when the isolated H atom is used as a reference). The energy difference between the high and low spin states is 0.34 eV for VH_1, it reduces then to 0.10 for VH_2; it is 0.13 eV for the vacancy.

It is interesting to compare these numbers with the energy of similar reactions performed on molecules, when the same functional (B3LYP) and basis set (6-21G) are used. For ternary carbon atoms (a carbon linked to one H and three C atoms, as in isobutane) E_H is 2.1 eV, then 1.05 eV higher than for VH_1^d. For secondary carbon atoms (the central carbon atom in

propane, for example) it increases by about 0.2 eV, and the same step is observed in going from secondary to primary carbon atoms (in ethane, for example). It turns then out that the C-H bond in VH_1 is much weaker than typical C-H bonds in molecules, and that the difference increases progressively when other H atoms are inserted in the vacancy. E_H is as large as 1.7 eV in VN_3H^{48}, larger then by 0.6 eV than in VH_1.

Table II reports, for comparison, also the defect formation energy (E_f) obtained according to

$$nC + \frac{x}{2}H_2 \leftrightharpoons VH_x \tag{8}$$

where nC is a cell of pristine diamond containing n carbon atoms. The trends along the series are obviously parallel to the ones for E_H; the formation energies turn out to the strongly hendothermic, due to the high stability of the starting compounds, *ie* diamond and H_2 molecules.

B. Spectroscopic characterization

The IR and Raman spectra of pristine diamond are very simple: the former is completely flat, the latter is characterized by a single peak at 1332 cm^{-1} (the calculated one with the present functional and basis set is at 1317 cm^{-1}, 15 cm^{-1} below the experiment). The IR and Raman spectra of the pure vacancy V show some structure below the 1317 diamond Raman peak (two intense peaks at 1106 and 1301 cm^{-1} are the main features), whereas no peak appears above.[46] All peaks in the high wavenumber interval (say 1332-5000 cm^{-1}) must be thus attributed to the presence of hydrogen in our simulation (or possibly also to other kind of defects in experiments). We start our analysis from Figure 4, that shows the full IR spectra of the four systems (and six states) we are interested here. The spectra are obtained with the 64 atoms supercell; as in each panel the maximum is determined by a peak whose height can differ by a large amount from the others, a different scale is used in each panel. At the same time, in order to avoid the complete crush of many of the features of the spectra, the highest peak has been truncated properly, as indicated in the figures. The most striking feature emerging from the comparison of the six figure is the huge difference in the intensity scale, that can reach 232 km/mol in VNH_1^d and 432 km/mol in VNH_1^q (this state turns out however to be 0.32 eV less stable than the doublet, so it is hardly observed in standard conditions). In VH_2^s the scale is two orders of magnitude smaller than in VH_1,

whereas in VH_2^t it is one order of magnitude larger. In VH_3^s the maximum is 90 km/mol, and in VH_4 it is 5 times smaller.

If we focus however our attention on the bending and stretching modes that emerge from the pure diamond manifold (say modes above 1330-1350 cm^{-1}), and can then be clearly identified, and disregard the excited spin states (VH_1^q and VH_2^t), the situation is the following (see also Table IV):

- In VH_1^d only one bending mode is visible, at 1421 cm^{-1} with intensity of 230 km/mol (the intensity of the other bending mode at 1487 cm^{-1} is negligible, only 4 km/mol). The stretching mode at 3188 cm^{-1} is very intense (935 km/mol).

- In VH_2^s there are two bending modes above 1350 cm^{-1}, one at 1602, the other at 1399 cm^{-1}, the first with medium, the second with low intensity (64 and 26 km/mol, respectively). The two stretching modes at 3605 and 3404 cm^{-1} have very low intensity (9 and 16 km/mol).

- Also in VH_3^d there are two C-H bending modes above 1350 cm^{-1}, at 1530 and 1485 cm^{-1}, both with medium-low intensity (55 and 32 km/mol). The symmetric stretching mode at 3909 has very low intensity (33 km/mol); the antisymmetric one, at 3647 cm^{-1} is extremely intense (1148 km/mol).

- In VH_4 one bending mode at 1491 (three times degenerate) is very intense (224 km/mol); the other bending mode at 1408 cm^{-1}, shown in Table IV and twofold degenerate, is silent due to symmetry together with the totally symmetric stretching at 4239 cm^{-1}. The second one, at 3980 cm^{-1}, has negligible intensity.

In a hypothetical diamond sample containing the four defects at the same concentration, thus, two peaks would dominate the bending region: the first one is at 1421 (VH_1^d), the second at 1491 (VH_4) cm^{-1} and with about the same intensity.Also in the stretching region two peaks dominate: one at 3188 (again VH_1^d) and one at 3647 cm^{-1} (VH_3^d), with intensities that are 4 to 5 times larger than the largest one in the bending region. Looking at Figure 5, top, in which this hypotetical spectrum in the high wavenumber region and referring to the S_{64} supercell is reported, it is evident that VH_2 and VH_4 are not visible in the stretching region.

Before leaving this part of the discussion, we can try to answer to the three following

13

questions:

I) are there other bending modes related to H?

II) are the wavenumbers here reported stable with respect to the defect dilution?

III) is the Raman spectrum giving more visibility to the systems that are essentially absent from the high wavenumber region of the IR spectrum, namely VH_2^s and VH_4?

As regards the first question, in a sort of single particle approximation, that works reasonably well when hydrogen is involved, due to its small mass, one would expect three modes per H atom. Looking at Table IV, we discover that all the stretching modes are reported (the degeneracy should be taken into account), whereas a certain number of bending modes are lacking: 3 in VH_4 and VH_3, and two in the two spin states of VH_2. Symmetry analysis, combined with the graphical animation of the modes, can help to identify the position of the "lacking" modes. For VH_4 the threefold degenerate modes at 347 cm^{-1}, of F_1 symmetry, both IR and Raman inactive, complete the set of bending modes. For VH_3 the twofold degenerate modes at 450 cm^{-1}, of E symmetry, and the one at 442 cm^{-1}, of A_2 symmetry, complete the set. For VH_2^s the modes at 483 and 1352 cm^{-1}, both of B" symmetry, complete the set.

As regards the second question, we open now a small discussion concerning the stability of the numbers just discussed when the size of the supercell is varying when the VH_4 system is considered. The high wavenumbers part of the IR spectrum generated with the four cubic supercells ($\vec{a}=\vec{b}=\vec{c}$ and $\alpha = \beta = \gamma = 90°$) containing 64, 216, 512, 1000 atoms are shown in Figure 8. The Figure permits to answer to two related questions, namely a) how is changing the IR spectrum with the defect concentration? and b) can we be sure that the differences are due to the different defect dilution and not, at least in part, to the different numerical errors accumulating for different sizes of the supercell?

As regards the second question, two evidences can be mentioned, referring to perfect systems, investigated with increasing supercells (in these cases obviously different supercells must provide the same frequencies and intensities): I) when the vibrational spectrum of perfect diamond is produced with supercells including an increasing number of atoms, from 2 to 1024, the Raman peak at 1317 moves by no more than 1 cm^{-1}. II) Baima et $al.$[25], in a paper devoted to the thermodynamics and phonon dispersion of pyrope and grossular, performed vibrational calculations with the CRYSTAL code on unit cells containing from 80 to 2160 atoms. The wavenumbers at the Γ point show a maximum difference of only 0.357 cm^{-1}

(Table 1 in the paper mentioned above). Figure 8 provides additional evidence for point a), and an answer to point b). In short: the peak position in the S_{216} cell, differs by 1, 3 and 8 cm^{-1} with respect to S_{1000}; for S_{512} the difference reduces to 5, 1 and 2 cm^{-1}; also the intensities, that vary from 240 to 2 km/mol, are extremely stable from S_{216} on. We can conclude that the 3 indicated peaks still vary by some amount from S_{64} to larger cells as a consequence of the defect-defect interaction; from S_{216} on, the differences might also depend in part from negligibly small numerical noises of the code.

The answer to the last question can be found in Figure 7, where the high frequency part of the harmonic Raman spectrum is shown. The intensities provide a couple of surprises (the wavenumbers are obviously the same as for the IR spectrum): a) the symmetric VH$_4$ peak has now non null intensity; b) all the seven peaks have intensities that differ by no more than 30%, so that in the Raman spectrum all the 4 H occupations should be visible at variance with respect to IR.

C.   The anharmonic treatment of the CH bending and stretching.

Table V reports the results of the numerical solution of the one-dimensional Schrödinger equation along the C-H coordinate, as described in Subsection II B. In the last two colums also the harmonic frequency ω_H obtained by diagonalizing the Hessian matrix, and using the one point ω_H^1 or two points ω_H^2 formulas (see equations 2 and 3) are reported. Data refer to the S_{64} supercell. The convergence with the supercell size, not shown, is as quick as for the harmonic frequency shown in Figure 8. The B3LYP fundamental anharmonic wavenumber of VH$_1^d$ is at 3015 cm^{-1}, 217 cm^{-1} lower than the harmonic frequency (ω_e, at 3232 cm^{-1}, see Equations 5 and 6). It is worth noting that the C-H stretching of the VN$_3$H defect[48] is 120 cm^{-1} higher (3135 cm^{-1} at the same level of theory), whereas the one of the ternary carbon of isobutane (the C atom is linked to one H and three C atoms, a local situation similar to the one of VH$_1$) is about 150 cm^{-1} lower (2862 cm^{-1}). The anharmonicity of VH$_1^q$ is much larger than the d one: 335 vs 217 cm^{-1} (in VN$_3$H and isobutene it is much smaller: 138 and 116 cm^{-1}, respectively[48]). The difference between ω_e and ω_H (last column) is not surprising: when the energy surface is very anharmonic, as in the present case, the use of only two energy points (the equilibrium and one displaced to the right or to the left, as for ω_H) is not enough for an accurate estimate of the second

15

derivative in the minimum.

Frequency analysis of the four saturations:

All six studied systems have been approached calculating the anharmonic approximation and successively compared with the respective harmonic frequencies in order to obtain anharmonicity estimation. The anharmonic contributions have been evaluated as a function of the C-H stretching, resolving the one-dimensional Schrödinger equation. In this approach the carbon backbone of the cell is frozen, leaving free to move only the hydrogen atoms. Obviously this kind of anharmonic approximation provides a reasonable estimation only for the strenghing modes; in fact the stretching are strongly decorrelated respect to the other modes and stretching-bending coupling can be neglected introducing a variable error in the anharmonic evaluation. When more then one Hydrogen atoms is prensent, it is worth of note that the symmetric and anti-symmetric anharmonicity can be evaluated keeping or breaking the symmetry in C-H displacement; indeed in the former case the hydrogen atoms are moved simultaneously, reproducing a symmetrical behaviour, while in the latter case hydrogen atoms are moved one at a time, miming an anti-symmetric vibrations. The entity of the anharmonic shift is different in each cases: from 1 to 2 hydrogen atoms saturating the vacancy, we obtain a red shift.Whereas when there are 3 or 4 hydrogen atoms, saturating the vacancy, a blue shift has been observed. Usually the anharmonic contribution is more pronounced for the high spin state (quadruplet and triplet state), and in each case the symmetrical stretching have a bigger shift if is compared to the anti-symmetric. In VH_1 system, considering the anharmonic shift of the stretching modes, it can be found one vibration at 2797 cm^{-1} with an intensity of 82 km/mol for the doublet state and one at 2483 cm^{-1} with 256 km/mol intensity for the quadruplet state. The energy difference between the two states is 0.13 eV (Table II). The corresponding Boltzman population ratio between the quadruplet and doublet state at 298.15 K is 0.00634. This is roughly estimation because the dft-energy difference is computed at 0K and probably the effect of the temperature will populate the high spin state, increasing the Boltzmann ratio. These peaks represent the most intensive features in the IR spectrum. In attempt to match this feature with experimental work of Fritsh[4] we can explore the literature data in a range of /pm 20 cm-1 cm^{-1} respect to the theoretical values. Different signal follow in this frequencies range for the doublet state: the 2784(6) and 2798 cm^{-1} peaks attributed to the H in diamond type Ib[2] and the 2812 cm^{-1}

16

peak referred to hydrogen in cuboid sector of historical asteriated hydrogen-rich diamonds[49]. For the doublet it cannot find any signal; indeed in the range 1461-2784, in the experimental data, there is an empty region. In addition, the strong intensity of this peak, would make it clearly visible in the spectrum and since there is no trace, this aspect could be considered as an evidence of the absence of this defect. For the VH_2 system the difference in energy between the two spin states is 0.34 eV, this larger energy gap make the triplet state unpopulated (Boltzmann ratio of $1.8 \ 10^{-6}$), and so we have only considered the more stable state. This defect has a maximum intensity lower then the one hydrogen saturation case (1-7 km/mol). The symmetrical stretching of the low spin state, in anharmonic approximation, have one feature at 3552 cm^{-1}. The effect of anharmonic correction is stronger then the system with only one hydrogen, due to the steric repulsion of the hydrogen atoms in the vacancy cavity and in attempt to find a signal matching between the experiments and theoretical calculation the range of experimental frequencies centred to the theoretical spot must be enlarged. In a wider range of $/pm$ 50 cm^{-1} it is possible to find a signal at 3525 releted to (L. Massi:Etude des dfauts dans les diamants bruns et les diamants riches en hydrogne(PhD thesis, University of Nantes, France, 2006e)). The asymmetrical stretching shows one theoretical feature at 3378 cm^{-1}. This spot can be matched with one experimental features in $/pm$ 50 cm^{-1} range; indeed there are 3354 cm^{-1} signal refereed to [L. Massi: Etude des dfauts dans les diamants bruns et les diamants riches en hydrogne(PhD thesis, University of Nantes, France, 2006) (in French) In the VH_3 system the anharmonic symmetrical stretching (3943 cm^{-1}) and anti-symmetric (3653 cm^{-1}) stretching dont have any matching with experimental data; indeed in the experimental data there is a not populated region going from 3525 to 4167 cm^{-1}. The VH_4 system has the symmetrical stretching IR inactive for symmetry and the anti-symmetric follow at 4037 cm^{-1}, and it falls into the same vacuum region as described above.

IV. CONCLUSIONS

COPIA

In this work a series of defects consisting of hydrogen atoms populating the vacancy in diamond have been investigated (VH_y, y=1 to 4). Only the highest loading defect (VH_4) has a closed shell ground state. VH_1 can exist in the quadruplet and doublet spin states (three

uncoupled electrons), VH_2 in a triplet and singlet state, VH_3 only in the doublet state.

Two main issues have been considered in the present study:

i) are all the model here proposed realistic from the energetic point of view? Can they be inserted in the long list of defects in diamond?

ii) if they exist, are they also visible from the experimental point of view, in particular do they produce visible, intense IR peaks?

The answer to the first question is positive. If reference is done to the V defect, then the saturation with hydrogen of one of the carbon atoms surrounding the vacancy is an exothermic process, also in the less favourable case in which the H atom comes from H_2 and then requires to brake a strong covalent bond. The bonds with neighboring C atoms of the many H atoms floating around in diamond (for example in interstitial positions) is weaker than in H_2, and then the hydrogenation of V becomes more favourable.

As regards the second question, we focused here our attention on the CH stretching modes, that appear at wavenumbers much higher than 1340 cm^{-1}, and then far away from the Diamond+V+N manyfold, characterized by a superposition of vibrational bands that form essentially a continuum. The 10 stretching modes characterizing the systems here investigated span nearly 1000 cm^{-1}, and should be in principle detectable individually, so as to permit to identify unambiguously all these defects. However most of them do have a quite low intensity, so that they are hardly visible in the very rich IR experimental spectrum, to which many other kind of defects are probably contributing. The only one easily detectable in experiments is the peak at 3107 cm^{-1}, that has an intensity of 621 km/mol, and is now attributed unambiguously to the VN_3H defect.The second most intense peak has intensity of 346 km/mol (just a bit more than 50% the one of VN_3H), whereas the other 8 peaks span from 30 % (just one) of it, to nearly null intensity. It should be noticed that other defects can have quite high intensity, and then generate large bands that completely hidden the small peaks. For exmaple the stretching mode of VNH, whose anharmonic wavenumber is at xx, has intensity 0f 900 km/mol, then 50% higher than the more intense one of this set (we remind that the IR intensity can be evaluated in an absolute scale, so that cross comparison between different systems is possible also ina bsolute values. As a consequence of the previous discussion,we can conclude that many of the defects here investigated (actually,

ALL of them) can exists in defective diamond, but the evidence of their existence cannot be obtained for most of them from IR spectra.
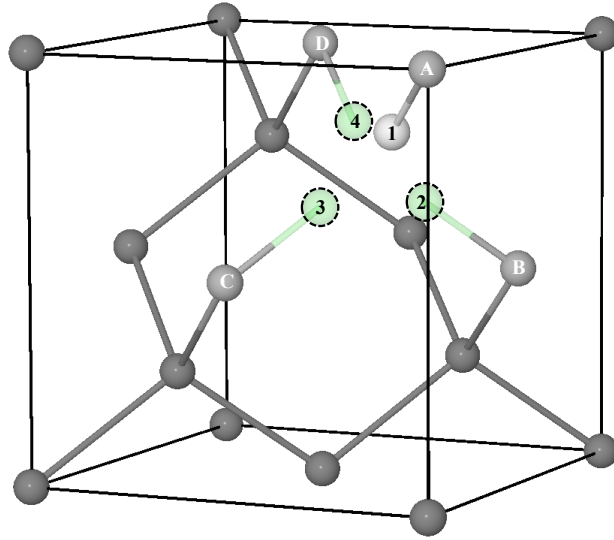
Figures

FIG. 1: A schematic representation of the VH_{1+n} (n=0, 1, 2 and 3) defects. Green positions can be either empty (VH_1) or occupied by hydrogen atoms (position 2 in VH_2, position 2 and 3 in VH_3; 2, 3 and 4 in VH_4).
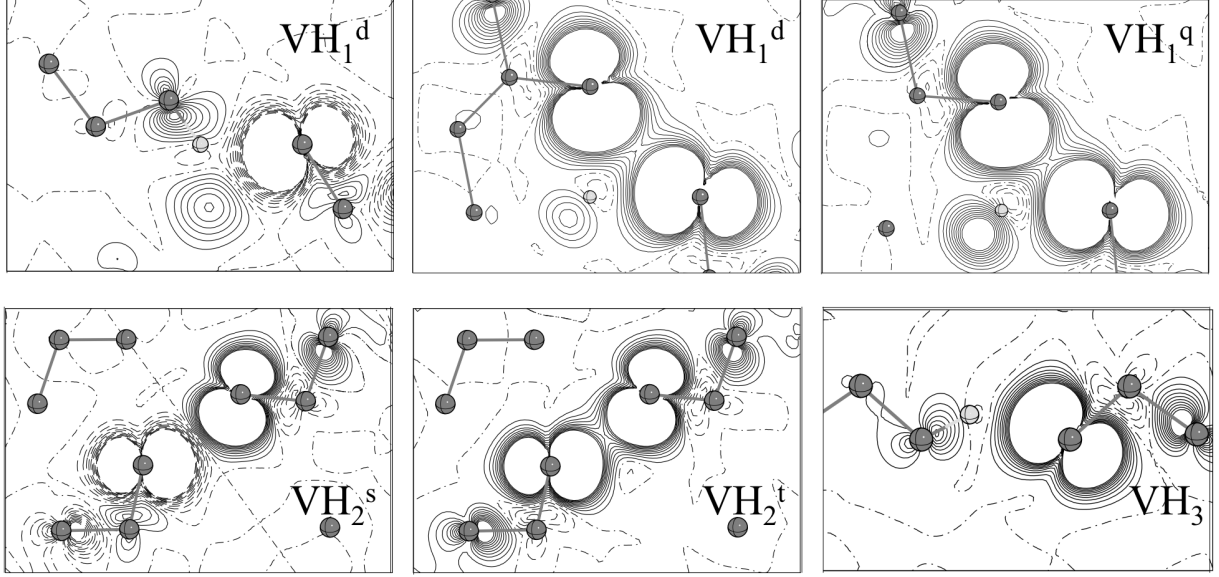
FIG. 2: Spin density maps of the VH_1^d (projected over two differents planes), VH_1^q, VH_2^s, VH_2^t and VH_3 defects. The three points defining the planes, in the case of VH_1^d system the plane in the first figure contains the carbon atoms with opposite spin orientations respect to the other two carbons. To the contrary in the second figure the plane contains the two carbon with same spin configuration. In the case of VH_2 system, are the two C and D (carbon atoms with the unpaired electrons) with the centre of the vacancy. They are represented in bottom panel. In the VH_3^d system (last immage in bottom panel) the plane has been defined by the D atom (the only carbon atom with an unpaired electron), hydrogen H_1 and carbon D. See Figure 1 for the labels of the atoms. Isodensity lines differ by 0.01 $|e|/(a_0)^3$; spin density is truncated at $\pm$ 0.1 $|e|/(a_0)^3$. Continuous, dashed and dot-dashed lines indicate positive, negative and zero values, respectively.
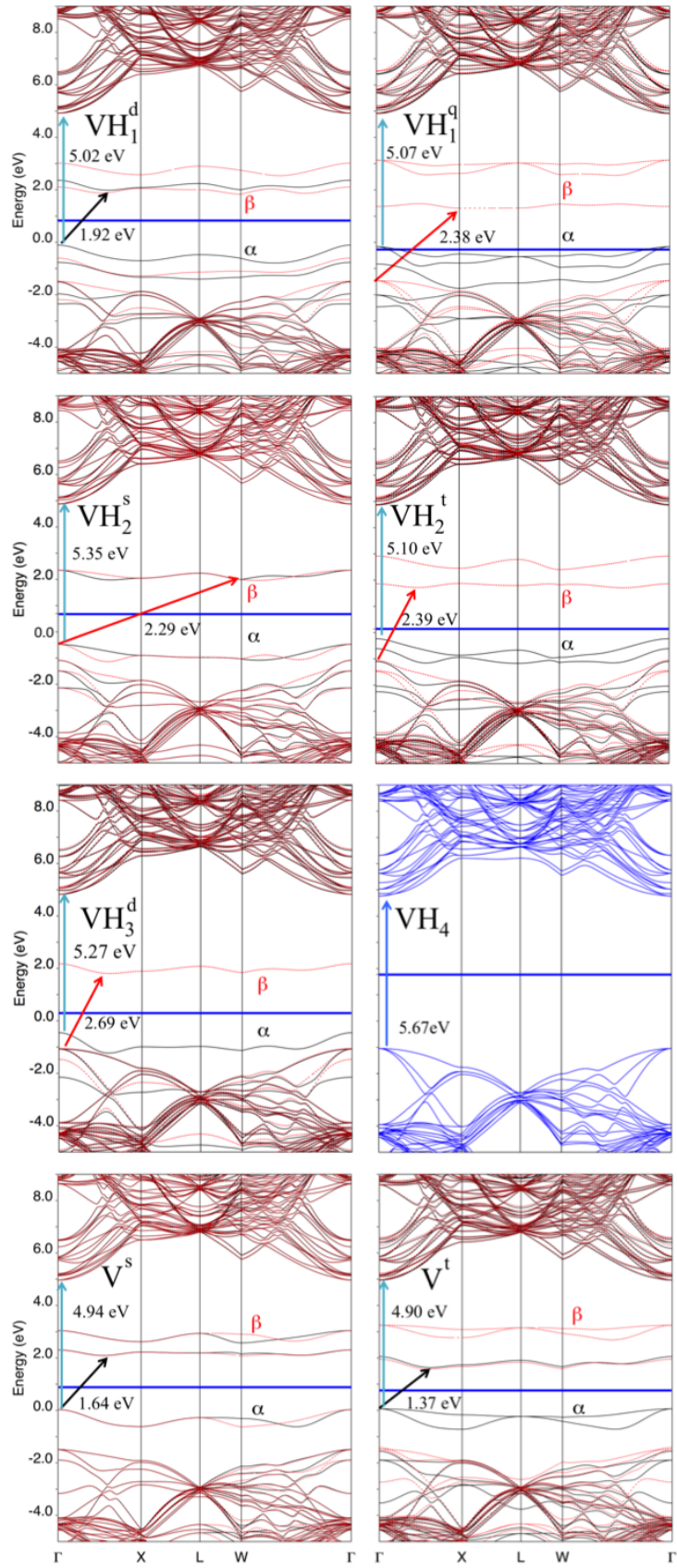
FIG. 3: Electronic band structure of the diamond vacancy with incremental hydrogen saturation. The top panels refer to the VH_1 quadruplet q (left) and doublet d (right) electronic states. The second row panels show the VH_2 triplet t (left) and singlet s (right) band structure. The third row panels refer to VH_3 in its d state, whereas VH_4, in its closed shell ground state, is shown to the right. The vacancy V^t (left) and V^s (right) states are also shown, for completeness, in the bottom panels. Black and red bands correspond to α and β electrons, respectively. The blue line is the Fermi level. Data obtained with the S_{64} supercell.

FIG. 4: Infrared spectra of the four VH_n (n=1 to 4) defects, in their various spin states, computed with the S_{64} supercell.

FIG. 5: Harmonic (top) and anharmonic (bottom) wavenumbers for the C-H stretching mode(s) for the VH_x defects. When more than one hydrogen atom is present there are two stretching modes (symmetric, at high wavenumber, and antisymmetric, at low wavenumber, and marked with an asterisk). The height of each bar is the simulated IR intensity evaluated at the harmonic level. Calculations refer to B3LYP/6-21G, and to the S_{64} supercell.

FIG. 6: Harmonic wavenumbers for the C-H bending modes for the VH_x defects. The height of each bar is the simulated IR intensity evaluated at the harmonic level. Calculations refer to B3LYP/6-21G, and to the S_{64} supercell.

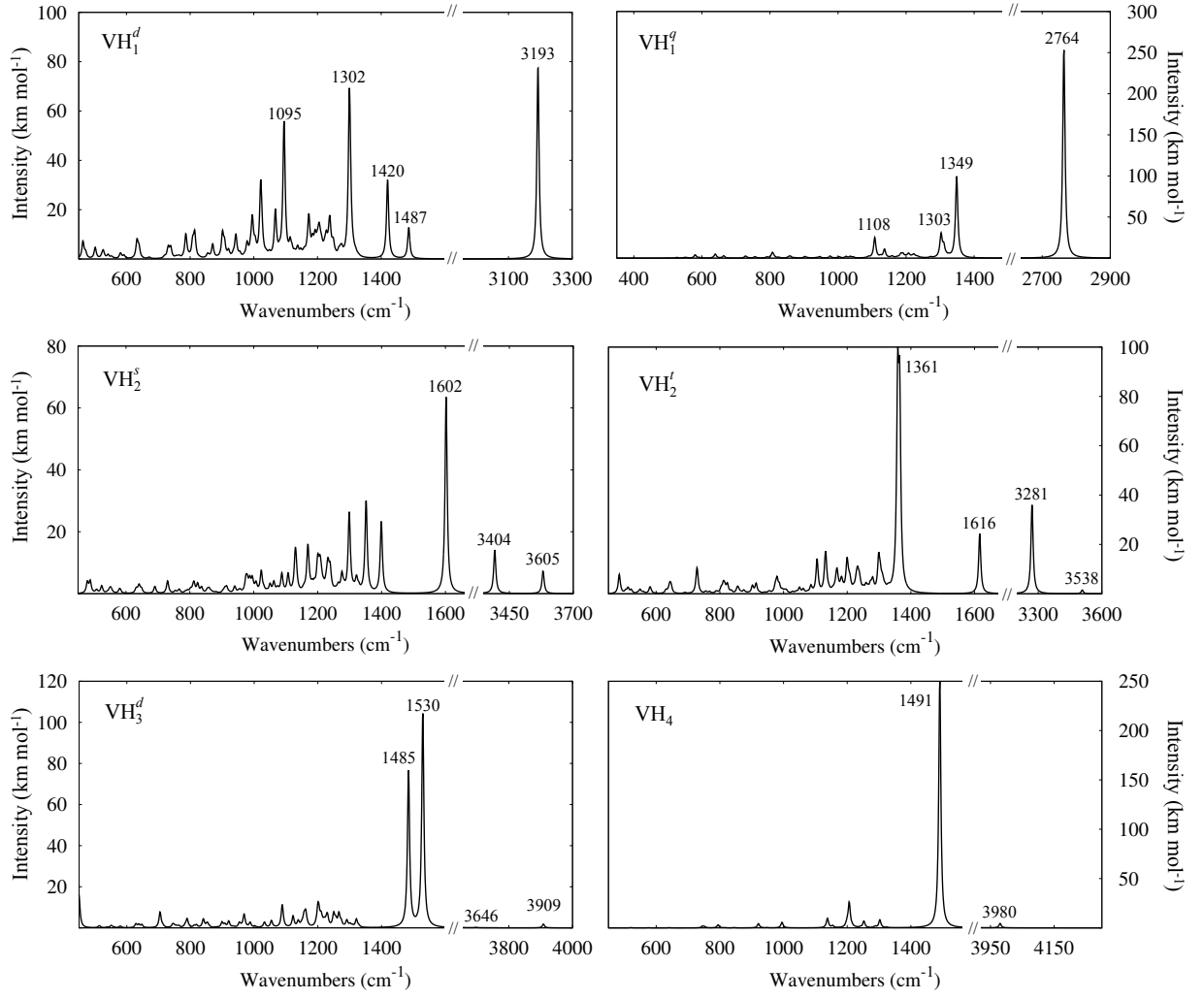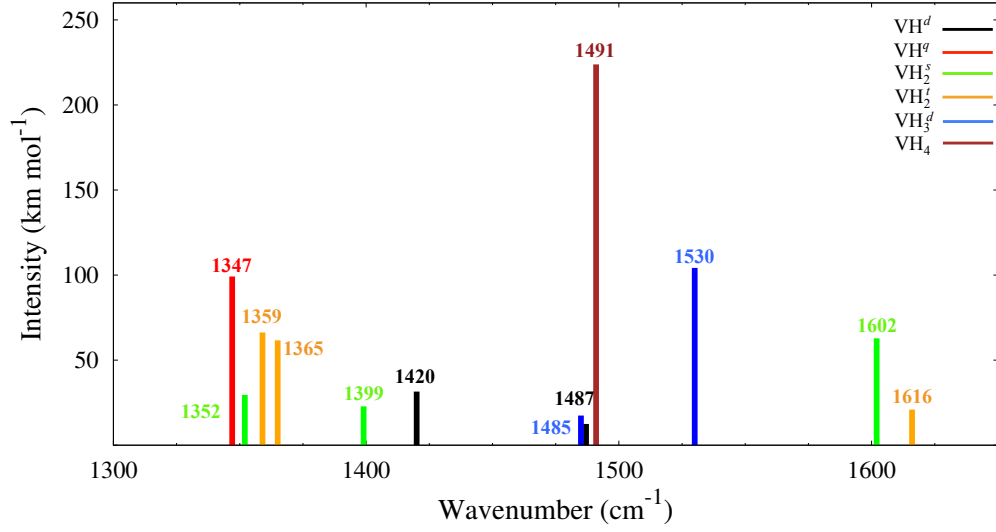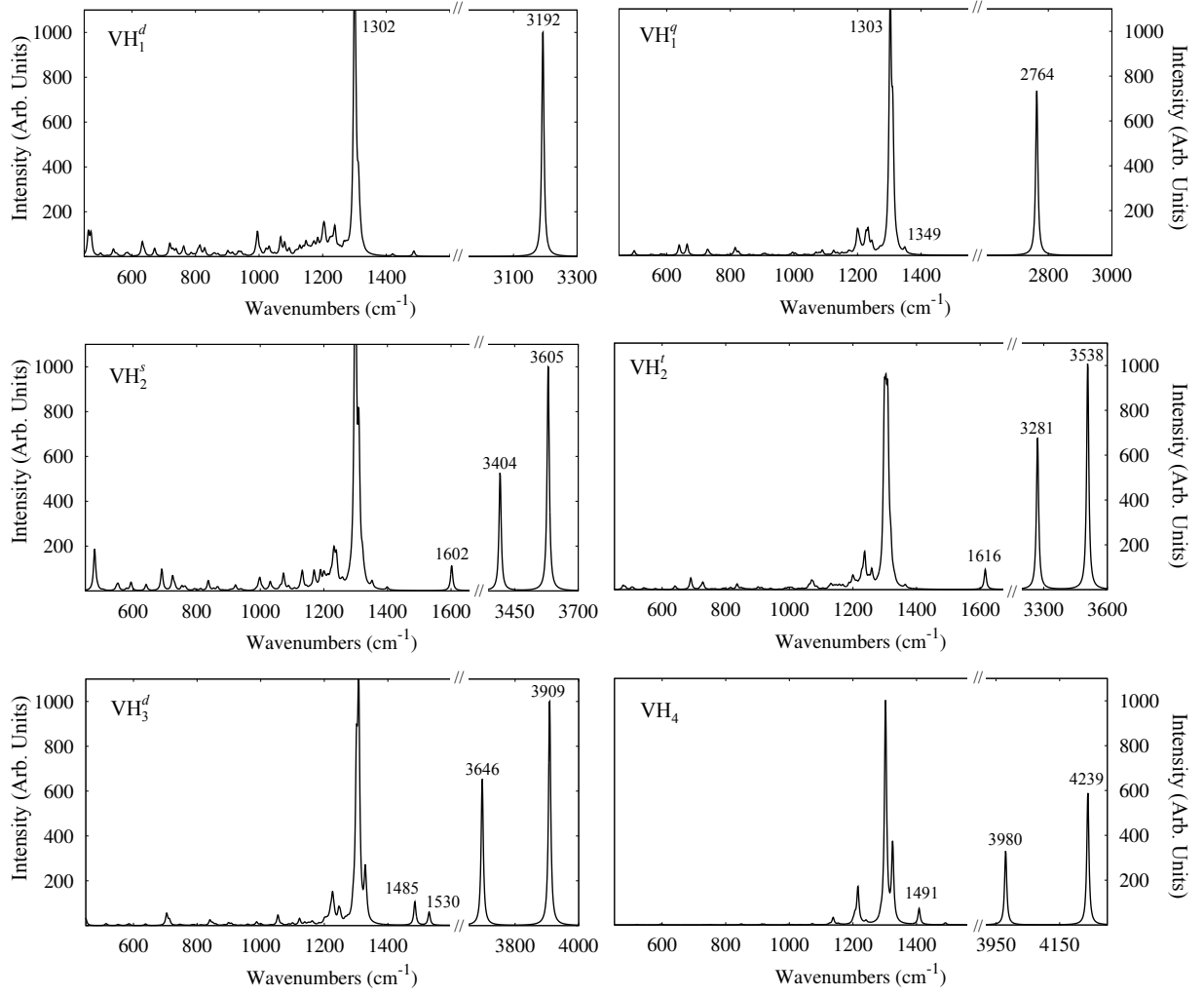FIG. 7: Simulated Raman spectra of the four VH_n ($n=1$ to 4) defects, in their various spin states, computed with the S_{64} supercell.
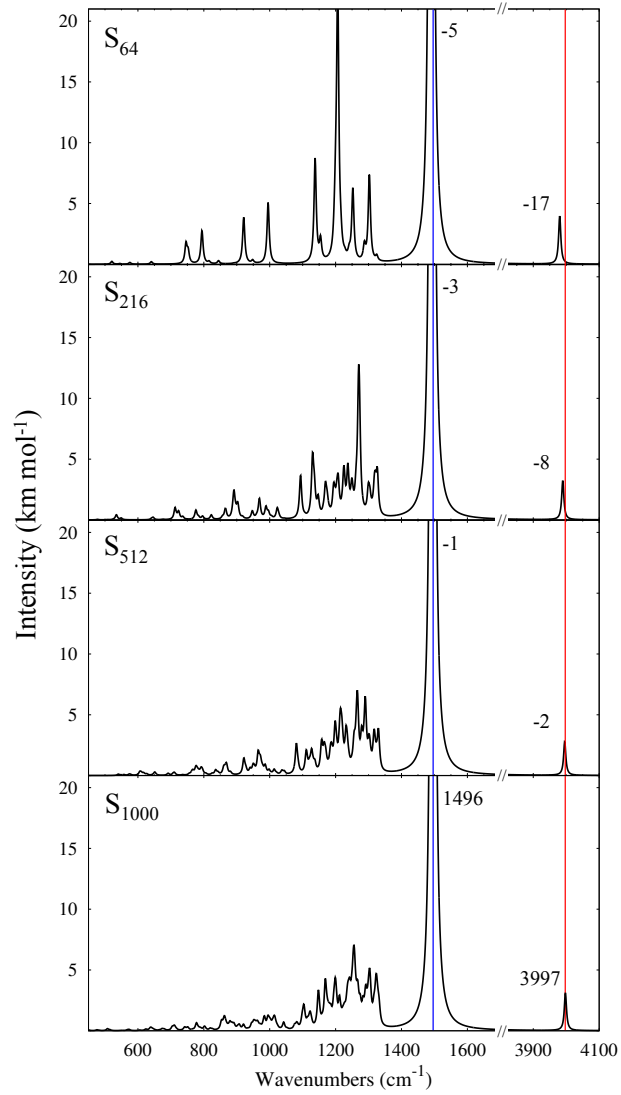
FIG. 8: The effect of the defects dilution on the computed IR spectrum of VH_4. Four supercells containing 64, 216, 512 and 1000 atoms are considered. Vertical blue and red lines mark the position of hydrogen bending and asymmetric stretching modes (both triply degenerate), respectively, for the S_{1000} case. Concerning S_{64}, S_{216}, and S_{512} cases, frequency shifts with respect to the S_{1000} (bottom figure) are reported.

Tables

System	R_{CH}	R_{HH}	Q_H	Q_{C1}	μ_H	μ_{C1}	B_{CH}	B_{HH}
VH_1^d	1.072	-	+0.17	-0.15	-0.01	+0.04	+0.27	-
VH_1^q	1.108	-	+0.18	-0.13	-0.02	+0.17	+0.26	-
VH_2^s	1.052	1.273	+0.17	-0.14	0.00	0.00	+0.30	-0.04
VH_2^t	1.059	1.277	+0.17	-0.13	-0.01	+0.07	+0.30	-0.04
VH_3^d	1.036	1.273	+0.12	-0.10	-0.00	+0.03	+0.31	-0.07
VH_4	1.017	1.251	+0.07	-0.04	-	-	+0.29	-0.10

TABLE I: Structural and Mulliken population data for the VH_x^y defects, where the y superscipt can be s (singlet), d (doublet), t (triplet) and q (quadruplet). In the case of closed shell states, the y superscript is absent. R_{CH} and R_{HH} are the shortest distances (in Å) between the indicated atoms, B_{CH} and B_{HH} are the corresponding bond populations, Q_X and μ_X are the net electronic charges and magnetic moments of atom X (B, Q and μ in $|e|$ units). All data refer to the S_{64} supercell.

	E_{VH_x}	E_H	E_f	δE
V^s	-2397.2713		-6.85	
V^t	-2397.2664			0.13
VH^d	-2397.8945	1.06	-5.79	
VH^q	-2397.8820	0.72	-6.13	0.34
VH_2^s	-2398.5054	1.78	-5.07	
VH_2^t	-2398.5015	1.67	-5.18	0.10
VH_3^d	-2399.1019	2.11	-4.74	
VH_4	-2399.6855	2.09	-4.76	

TABLE II: Homolytic dehydrogenation (E_H, in eV) and formation (E_f, in eV) energies of VH_x evaluated according to equations 7 and 8, respectively. δE (in eV) is the energy difference between the highest and lowest spin state (the former is more stable in all cases). The total energy of the various systems, in hartree, is also shown in the first column. The H energy, -0.5844 hartree, is half the energy of the H_2 molecule. The energy of the isolated H atom is 0.4969 eV. The pure diamond energy is -2435.58 hartree. Data refer to the S_{64} supercell.

Method	S_x	E_{H_2}	E_C^{64}	E_{V^s}	E_{VH_4}	E_G	E_H	E_f
B3LYP	S_{64}	-1.1687	-2435.5789	-2397.2713	-2399.6855	5.67	2.09	4.76
B3LYP	S_{128}	-1.1687	-4871.1578	-4832.8486	-4835.2591	5.71	1.99	4.90
HF	S_{64}	-1.1268	-2421.7608	-2383.6978	-2385.9704	11.79	0.51	5.55
PBE0	S_{64}	-1.1639	-2434.8068	-2396.4979	-2398.9123	5.77	2.36	4.86
HSE06	S_{64}	-1.1636	-2434.7622	-2396.4556	-2398.8676	5.13	2.31	4.86
PBE	S_{64}	-1.1620	-2434.4882	-2396.2049	-2398.6029	3.97	2.02	4.64
LDA	S_{64}	-1.1333	-2416.0004	-2377.9867	-2380.5056	3.96	6.87	0.31

TABLE III: Total (in hartree), homolytic dehydrogenation (E_H, in eV) and formation (E_f, in eV) energies of VH_4 obtained with various methods. E_{V^s} is the energy of the vacancy in the singlet state. E_H and E_f are obtained according to Equations 7 and 8, respectively. E_G is the band gap.

	Stretching				Bending			
	ω_{S_1}	I_{S_1}	ω_{S_2}	I_{S_2}	ω_{B_1}	I_{B_1}	ω_{B_2}	I_{B_2}
VH_1^d	3188 A$'$	82	-	-	1487 A$'$	13	1421 B$''$	32
VH_1^q	2797 A1	256	-	-	1356 E	106	-	-
VH_2^s	3605 A$'$	7	3404 B$''$	13	1602 A$^{i'}$	63	1399 A$'$	23
VH_2^t	3538 A1	1	3281 B1	31	1616 A1	21	1359 B2	62
VH_3^d	3909 A1	2	3647 E	0	1530 E	104	1485 A1	76
VH_4	4239 A1	0	3980 F2	4	1491 F2	224	1408 E	0

TABLE IV: Peak position (ω in cm^{-1}) and intensity (I in km/mol) of the C-H stretching (S) and bending (B; only the ones above 1350 cm^{-1} are shown) modes. The symmetry of the mode and are also reported and in the bracket there's the intensities of the peaks obtained using a Lorentzian fitting with FWHM of 8 cm^{-1}.

n H	PG	IR	N_v	ω_{e1}	ω_{e2}	$\omega_e\chi_e$	ω_e	$\delta\omega_{e1e}$	ω_H^1
VH_1^q	C_{3v}	A_1	1	2483	4631	168	2818	-335	2797
VH_1^d	σ_v	A'	1	3015	5814	108	3232	-217	3188
VH_2^t	C_{2v}	B_1	1	3253	6334	86	3426	-173	3281
VH_2^t	C_{2v}	A_1	2	3477	6897	28	3533	-56	3538
VH_2^s	σ_v	B''	1	3378	6617	70	3518	-140	3404
VH_2^s	σ_v	A'	2	3552	7050	27	3606	-54	3605
VH_3^d	C_{3v}	E	1	3653	7202	53	3759	-106	3647
VH_3^d	C_{3v}	A_1	3	3953	7921	-8	3938	15	3909
VH_4^s	T_d	F_2	1	4037	8021	27	4090	-53	3980
VH_4^s	T_d	A_1	4	4434	8952	-42	4349	85	4239

TABLE V: Harmonic and anharmonic C-H stretching (wavenumbers in cm^{-1}) for the various VH_n^i defects, where s,d,t and q superscripts stand for singlet, doublet, triplet and quadruplet. ω_{e1}, ω_{e2}, $\omega_e\chi_e$ and ω_e are obtained from the numerical solution of the one-dimensional Schroedinger equation, and are the fundamental anaharmonic contribution, the first overtone, the anharmonic constant and the fundamental harmonic frequency. N_v is the number of hydrogen atoms that are involved in the anharmonic motion. When larger than 1, all atoms are moving in phase. PG is the point group of the system in the selected state, IR is the irreducible representation according to which the system is vibrating. ω_H^1 and ω_H^2 are the harmonic frequencies obtained by diagonalizing the full hessian matrix, that is built by using the one point or the two point formula shown in equation 2 and 3 respectively. $\delta\omega_{e1e}$ is the difference between ω_{e1} and ω_e, the harmonic and anarmhonic wavenumbers, both computed by solving the one-dimensional Schroedinger equation.

1 Woods G. S and A. T. Collins. Infrared Absorption Spectra of Hydrogen Complexes in Type I Diamonds. *J. Phys. Chem. Solids*, 44(5):471–475, 1983.

2 T. Hainschwang, F. Notari, E. Fritsch, and L. Massi. Natural, Untreated Diamonds Showing the A, B and C Infrared Absorptions ("ABC Diamonds"), and the H_2 Absorption. *Diamond Relat. Mater.*, 15(10):1555–1564, 2006.

3 J. P. Goss, R. Jones, M. I. Heggie, C. P. Ewels, P. R. Briddon, and S. Öberg. Theory of Hydrogen in Diamond. *Phys. Rev. B*, 65(11):115207, 2002.

4 E. Fritsch, T. Hainschwang, L. Massi, and B. Rondeau. Hydrogen-Related Optical Centers in Natural Diamond: an Update. *New Diamond Frontier Carbon Technol.*, 17(2):63–89, 2007.

5 J. P. Goss, P. R. Briddon, V. Hill, R. Jones, and M. J. Rayson. Identification of the Structure of the 3107 cm^{-1} H-related Defect in Diamond. *J. Phys. Condens. Matter*, 26:145801, 2014.

6 J. J. Charette. Essai de Classification des Bandes d'Absorption Infrarouge du Diamant. *Physica*, 27(11):1061–1073, 1961.

7 C. E. Melton, A. A. Giardini, and C. A. Salotti. Observation of Nitrogen, Water, Carbon-Dioxide, Methane and Argon as Impurities in Natural Diamonds, 1972.

8 R. M. Chrenko, R. S. McDonald, and K. A. Darrow. Infrared spectra of diamond coat. *Nature*, 213:474–476, 1967.

9 J. P. Perdew and A. Zunger. Self-Interaction Correction to Density-Functional Approximations for Many-Electron Systems. *Phys. Rev. B*, 23(10):5048, 1981.

10 S. Salustro, F. Gentile, Ph. D'Arco, B. Civalleri, M. Rérat, and R. Dovesi. Hydrogen Atoms in the Diamond Vacancy Defect. A Quantum Mechanical Vibrational Analysis. *J. Chem. Phys.*, 15(10):1555–1564, 2006.

11 A. D. Becke. Density-Functional Thermochemistry. III. The Role of Exact Exchange. *J. Chem. Phys.*, 98(7):5648–5652, 1993.

12 C. Lee, W. Yang, and R. G. Parr. Development of the Colle-Salvetti Correlation-Energy Formula into a Functional of the Electron Density. *Phys. Rev. B*, 37(2):785, 1988.

13 R. Dovesi, R. Orlando, A. Erba, C. M. Zicovich-Wilson, B. Civalleri, S. Casassa, L. Maschio, M. Ferrabone, M. De La Pierre, P. D'Arco, Y. Noël, M. Causà, M. Rérat, and B. Kirtman. CRYSTAL14: A Program for the Ab Initio Investigation of Crystalline Solids. *Int. J. Quantum*

Chem., 114:1287, 2014.

[14] W. J. Hehre, R. Ditchfield, and J. A. Pople. SelfConsistent Molecular Orbital Methods. XII. Further Extensions of GaussianType Basis Sets for Use in Molecular Orbital Studies of Organic Molecules. *J. Chem. Phys.*, 56(5):2257–2261, 1972.

[15] M. M. Francl, W. J. Petro, W. J. Hehre, J. S. Binkley, M. S. Gordon, D. J. DeFrees, and J. A. Pople. Self-Consistent Molecular Orbital Methods. XXIII. A Polarization-Type Basis Set for Second-Row Elements. *J. Chem. Phys.*, 77(7):3654–3665, 1982.

[16] P. Dirac. A Theory of Electrons and Protons. *Proc. R. Soc. A*, 126(801):360–365, 1930.

[17] J. P. Perdew, K. Burke, and M. Ernzerhof. Generalized Gradient Approximation Made Simple. *Phys. Rev. Lett.*, 77(18):3865–3868, 1996.

[18] C. Adamo and V. Barone. Toward Chemical Accuracy in the Computation of NMR Shieldings: the PBE0 Model. *Chem. Phys. Lett.*, 298(1):113–119, 1998.

[19] A. V. Krukau, O. A. Vydrov, A. F. Izmaylov, and G. E. Scuseria. Influence of the Exchange Screening Parameter on the Performance of Screened Hybrid Functionals. *J. Chem. Phys.*, 125(22):224106–224106, 2006.

[20] R. Dovesi, V. R. Saunders, C. Roetti, R. Orlando, C. M. Zicovich-Wilson, F. Pascale, B. Civalleri, K. Doll, N. M. Harrison, I. J. Bush, Ph. D'Arco, and M. Llunell. *CRYSTAL 2014 User's Manual*. University of Torino, Torino, 2013.

[21] F. Pascale, C. M. Zicovich-Wilson, F. Lòpez Gejo, B. Civalleri, R. Orlando, and R. Dovesi. The Calculation of the Vibrational Frequencies of the Crystalline Compounds and its Implementation in the CRYSTAL Code. *J. Comput. Chem.*, 25(6):888–897, 2004.

[22] C. M. Zicovich-Wilson, F. Pascale, C. Roetti, V. R. Saunders, R. Orlando, and R. Dovesi. Calculation of the Vibration Frequencies of α-Quartz: The Effect of Hamiltonian and Basis Set. *J. Comput. Chem.*, 25(15):1873–1881, 2004.

[23] A. Erba, M. Ferrabone, R. Orlando, and R. Dovesi. Accurate Dynamical Structure Factors from *Ab Initio* Lattice Dynamics: the Case of Crystalline Silicon. *J. Comput. Chem.*, 34:346–354, 2013.

[24] C. Carteret, M. De La Pierre, M. Dossot, F. Pascale, A. Erba, and R. Dovesi. The Vibrational Spectrum of $CaCO_3$ Aragonite: a Combined Experimental and Quantum-Mechanical Investigation. *J. Chem. Phys.*, 138(1):014201, 2013.

[25] J. Baima, M. Ferrabone, R. Orlando, A. Erba, and R. Dovesi. Thermodynamics and phonon

dispersion of pyrope and grossular silicate garnets from ab initio simulations. *Phys. Chem. Minerals*, 43:137–149, 2016.

26 F. Pascale, C. M. Zicovich-Wilson, R. Orlando, C. Roetti, P. Ugliengo, and R. Dovesi. Vibration Frequencies of $Mg_3Al_2Si_3O_{12}$ Pyrope. An *Ab Initio* Study with the CRYSTAL Code. *J. Phys. Chem. B*, 109(13):6146–6152, 2005.

27 F. Pascale, P. Ugliengo, B. Civalleri, R. Orlando, Ph. DArco, and R. Dovesi. Hydrogarnet Defect in Chabazite and Sodalite Zeolites: A Periodic Hartree–Fock and B3-LYP Study. *J. Chem. Phys.*, 117(11):5337–5346, 2002.

28 R. Orlando, F. J. Torres, F. Pascale, P. Ugliengo, C. M. Zicovich-Wilson, and R. Dovesi. Vibrational Spectrum of Katoite $Ca_3Al_2[(OH)_4]_3$: a Periodic *Ab Initio* Study. *J. Phys. Chem. B*, 110:692–701, 2006.

29 F. Pascale, S. Tosoni, C. M. Zicovich-Wilson, P. Ugliengo, R. Orlando, and R. Dovesi. Vibrational Spectrum of Brucite $Mg(OH)_2$: a Periodic *Ab Initio* Quantum Mechanical Calculation Including OH Anharmonicity. *Chem. Phys. Lett.*, 396:308–315, 2004.

30 S. Tosoni, F. Pascale, P. Ugliengo, R. Orlando, V. R. Saunders, and R. Dovesi. Quantum Mechanical Calculation of the OH Vibrational Frequency in Crystalline Solids. *Molecular Physics*, 103(18):2549–2558, 2005.

31 R. Demichelis, Y. Nöel, B. Civalleri, C. Roetti, M. Ferrero, and R. Dovesi. The Vibrational Spectrum of α-AlOOH Diaspore: an *Ab Initio* Study with the CRYSTAL Code. *J. Phys. Chem. B*, 111(31):9337–9346, 2007.

32 M. Mérawa, P. Labeguerie, P. Ugliengo, K. Doll, and R. Dovesi. The Structural, Electronic and Vibrational Properties of LiOH and NaOH: an *Ab Initio* Study. *Chem. Phys. Lett.*, 387(4):453–459, 2004.

33 P. Ugliengo, F.Pascale, M. Merawa, P. Labéguerie, S. Tosoni, and R. Dovesi. Infrared Spectra of Hydrogen-Bonded Ionic Crystals: *Ab Initio* Study of $Mg(OH)_2$ and β-$Be(OH)_2$. *J. Phys. Chem. B*, 108(36):13632–13637, 2004.

34 G. M. Barrow. *Introduction to molecular spectroscopy*. McGraw-Hill, New York, 1962.

35 B. A. Hess, L. J. Schaad, P. Carsky, and R. Zahradnik. *Ab Initio* Calculations of Vibrational Spectra and Their Use in the Identification of Unusual Molecules. *Chem. Rev*, 86:709–730, 1986.

36 L. Maschio, B. Kirtman, R. Orlando, and M. Rérat. Ab initio Analytical Infrared Intensities for Periodic Systems Through a Coupled Perturbed Hartree-Fock/Kohn-Sham Method. *J. Chem.*

Phys., 137(20):204113, 2012.

[37] L. Maschio, B. Kirtman, M. Rérat, R. Orlando, and R. Dovesi. Comment on "*Ab Initio* Analytical Infrared Intensities for Periodic Systems Through a Coupled Perturbed Hartree-Fock/Kohn-Sham Method" [J. Chem. Phys. 137, 204113 (2012)]. *J. Chem. Phys.*, 139:167101, 2013.

[38] L. Maschio, B. Kirtman, M. Rérat, R. Orlando, and R. Dovesi. *Ab Initio* Analytical Raman Intensities for Periodic Systems Through a Coupled Perturbed Hartree-Fock/Kohn-Sham Method in an Atomic Orbital Basis. I. Theory. *J. Chem. Phys.*, 139(16):164101, 2013.

[39] L. Maschio, B. Kirtman, M. Rérat, R. Orlando, and R. Dovesi. *Ab initio* Analytical Raman Intensities for Periodic Systems Through a Coupled Perturbed Hartree-Fock/Kohn-Sham Method in an Atomic Orbital Basis. II. Validation and Comparison with Experiments. *J. Chem. Phys.*, 139:164102, 2013.

[40] M. Ferrero, M. Rérat, R. Orlando, and R. Dovesi. The Calculation of Static Polarizabilities of Periodic Compounds. The Implementation in the CRYSTAL code for 1D, 2D and 3D systems. *J. Comput. Chem.*, 29:1450–1459, 2008.

[41] M. Ferrero, M. Rérat, R. Orlando, and R. Dovesi. Coupled Perturbed Hartree-Fock for Periodic Systems: the Role of Symmetry and Related Computational Aspects. *J. Chem. Phys.*, 128:014110, 2008.

[42] D. A. McQuarrie and J. D. Simon. *Physical Chemistry. A Molecular Approach.* University Science Books, Sausalito, CA, 1977.

[43] J. L. Duncan, D. C. McKean, I. Tortoand A. Brown, and A. M. Ferguson. Infrared Studies of CH and CD Stretching Anharmonicity. *Journal of the Chemical Society, Faraday Transactions 2: Molecular and Chemical Physics*, 84(9):1423–1442, 1988.

[44] M. L. Myrick, A. E. Greer, A. A. Nieuwland, R. J. Priore, J. Scaffidi, D. Andreatta, and P. Colavita. Birge–Sponer Estimation of the C–H Bond Dissociation Energy in Chloroform Using Infrared, Near-Infrared, and Visible Absorption Spectroscopy. An Experiment in Physical Chemistry. *J. Chem. Educ*, 85(9):1276, 2008.

[45] P. Ugliengo. ANHARM. A Program to Solve Monodimensional Nuclear Schroedinger Equation. *unpublished*, 1989.

[46] J. Baima, A. Zelferino, P. Olivero, A. Erba, and R. Dovesi. Raman Spectroscopic Features of the Neutral Vacancy in Diamond from *Ab Initio* Quantum-mechanical Calculations. *Phys. Chem. Chem. Phys.*, 18(3):1961–1968, 2016.

[47] Alessandro Zelferino, Simone Salustro, Jacopo Baima, Valentina Lacivita, Roberto Orlando, and Roberto Dovesi. The electronic states of the neutral vacancy in diamond: a quantum mechanical approach. *Theor. Chem. Acc.*, 135(3):1–11, 2016.

[48] F. Gentile, S. Salustro, M. Causá, A. Erba, P. Carbonniére, and R. Dovesi. The VN_3H Defect in Diamond. A Quantum Mechanical Investigation of the Structural, Electronic and Vibrational Properties. *Phys. Chem. Chem. Phys.*, 111(44):11205–11213, 2017.

[49] Benjamin Rondeau, Emmanuel Fritsch, Michel Guiraud, Jean-Pierre Chalain, and Franck Notari. Three Historical "Asteriated" Hydrogen-Rich Diamonds: Growth History and Sector-Dependent Impurity Incorporation. *Diamond and Related Materials*, 13(9):1658 – 1673, 2004.